Journal of King Saud University – Science 33 (2021) 101417

Contents lists available at ScienceDirect

Journal of King Saud University – Science

journal homepage: www.sciencedirect.com

Original article

Effect of different supports for copper as catalysts on glycerol hydrogenolysis to 1,2-propanediol

Norsahida Azri [a,b], Ramli Irmawati [a,b,d,*], Usman Idris Nda-Umar [a,c], Mohd Izham Saiman [a,b], Yun Hin Taufiq-Yap [a,b,e]

[a] Department of Chemistry, Faculty of Science, Universiti Putra Malaysia, 43400 UPM Serdang, Selangor, Malaysia
[b] Catalysis Science and Technology Research Centre (PutraCAT), Faculty of Science, Universiti Putra Malaysia, 43400 UPM Serdang, Selangor, Malaysia
[c] Department of Chemical Sciences, Federal Polytechnic, PMB 55 Bida, Niger State, Nigeria
[d] Laboratory of Processing and Product Development, Institute of Plantation Studies, Universiti Putra Malaysia, 43400 UPM Serdang, Selangor, Malaysia
[e] Faculty of Science and Natural Resources, Universiti Malaysia Sabah, 88400 Kota Kinabalu, Sabah , Malaysia

ARTICLE INFO

Article history:
Received 14 November 2020
Revised 16 March 2021
Accepted 20 March 2021
Available online 27 March 2021

Keywords:
Copper
Comparison support
Acidity
1,2-PDO
Hydrogenolysis

ABSTRACT

In this work, several copper supported catalysts, Cu/Dol, Cu/Al_2O_3, Cu/Bent, Cu/Mont, and Cu/Talc were prepared using wet impregnation route and characterized using BET, BJH, XRD, H_2-TPR, NH_3–TPD, and SEM analytical techniques and subsequently tested in hydrogenolysis of glycerol to 1,2-propanediol (1,2-PDO). The nature of support was found to determine the activation of the catalysts. Among the tested catalysts, dolomite supported copper catalyst (Cu/Dol) exhibited superior performance due to the copper and dolomite species mutual interaction. The findings from the various characterization tests showed that the presence of copper species were essentially enriched on the dolomite grain surfaces, the redox properties, and acidic property of the catalyst enhanced, as well as the formation of the small size of the catalyst (Cu/Dol) contributed to the high conversion of glycerol (78.5%) and high 1,2-PDO selectivity (79%) with low methanol production as the by-product at 200 °C, 4 MPa H_2 and 10 h reaction conditions.

1. Introduction

Catalytic hydrogenolysis of glycerol into valuable 1,2-PDO, also known as propylene glycol (PG) from glycerol as by-product of biodiesel production is of paramount research interest due to its industrial importance. 1,2-PDO has been typically used in manufacturing of pharmaceuticals, cosmetics, food, as engine coolant, de-icing agent, and raw material for polyester resins (Liu et al., 2019). Considerable works have been devoted to the catalytic glycerol hydrogenolysis to 1,2-PDO (Soares et al., 2016). Many heterogeneous catalysts have been established to perform an active role in glycerol hydrogenolysis reaction. The use of low-priced transition metals as based catalysts In particular, copper-based catalysts have been highlighted with high catalytic performance, thus recommended as the most promising catalyst due to its capability in producing high 1,2-PDO. This was due its ability to highly react with the C-O bond while simultaneously inhibit the C–C bond cleavage towards side products with lower carbon (Freitas et al., 2018; Putrakumar et al., 2015). It was described that glycerol is selectively would be dehydrated to give acetol as the intermediate product on acid sites of the catalyst then proceeded by subsequent hydrogenation of acetol intermediate to 1,2-PDO (on metal sites) as illustrated in Scheme 1 (Mallesham et al., 2016). Thus, the addition of copper-based catalyst with acidic support could influenced the reaction system due to good copper and support interaction. Therefore, a catalyst with bifunctional sites (acidic and metal) was attempted to predominantly catalyze the hydrogenolysis of glycerol reaction. In the present work, the hydrogenolysis of glycerol was investigated over a series of Cu-supported catalysts (Cu/Dol, Cu/Al_2O_3, Cu/Bent, Cu/Mont, and Cu/Talc), with a metal copper loading of 20 wt% prepared via method of wet impregnation.

* Corresponding author at: Department of Chemistry, Faculty of Science, Universiti Putra Malaysia, 43400 UPM Serdang, Selangor, Malaysia.
E-mail address: irmawati@upm.edu.my (R. Irmawati).
Peer review under responsibility of King Saud University.

Production and hosting by Elsevier

https://doi.org/10.1016/j.jksus.2021.101417
1018-3647/

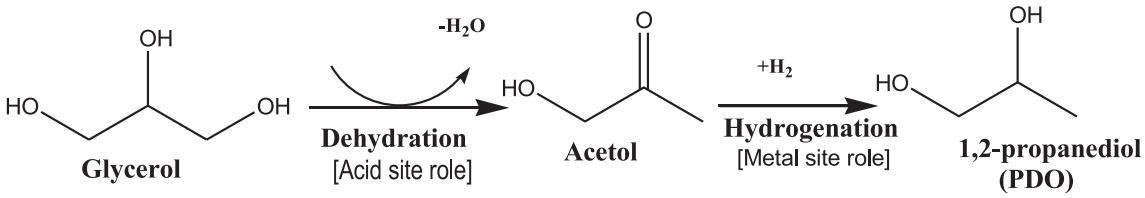

Scheme 1. Glycerol hydrogenolysis reaction pathway (Mallesham et al., 2016).

2. Experimental

2.1. Materials

For support materials, alumina (Al_2O_3), bentonite (Bent) and montmorillonite (Mont) were supplied from Sigma-Aldrich. Talcum (Talc) was obtained from commercial talcum powder (Johnson Brand). The mineral dolomite was obtained from Malaysia Dolomite Industries. Copper nitrate hexahydrate ($Cu(NO_3)_2{\cdot}6H_2O$) (≥99%) was purchased from Malaysia R&M Company. Glycerol (≥99.5%) used as reactant was supplied from Sigma-Aldrich.

2.2. Catalysts preparation

All Cu-supported catalysts were synthesized via wet impregnation method. Copper loading was fixed at 20 wt% for all the catalysts. In a typical synthesis, 3.8 g of copper nitrate hexahydrate was dissolved in 10 ml distilled water and was then poured into a 4 g support powder. The mixture was then stirred using a magnetic stirrer at 300 rpm and dried for about 3 h with heating at 90 °C on a hot plate. The dried mixture was then further aged for 24 h in the oven at 120 °C. Then the catalyst was undergo calcination process at 500 °C for 3 h in a tube furnace under static air with 10 °C/min heating rate to remove all the nitrates salt present in the catalysts. Next, the calcined catalysts were reduced by 5% H_2/Ar at 600 °C for 3 h under 2 °C/min rate in the same tube furnace. The synthesized catalysts were denoted as Cu/S (S = Al_2O_3, Bent, Mont, Talc, or Dol).

2.3. Catalyst characterization

The detail and procedure for catalyst characterization used in this study are similar to the one described in our previous report (Azri et al., 2020).

2.4. Catalytic reaction set up

The experiment of glycerol hydrogenolysis reaction conducted in this study was similar by the our published paper (Azri et al., 2020).

2.5. Product analysis

The procedure for product analysis performed in this paper are similar with Azri et al. (2020).

3. Results and discussion

3.1. Textural properties

The textural properties of all catalysts are listed in Table 1. The BET specific surface area value of Cu/Dol, Cu/Al_2O_3, Cu/Bent, Cu/Mont, and Cu/Talc was found to be 9.7 m^2g^{-1}, 34.5 m^2g^{-1}, 5.3 m^2g^{-1}, 30 m^2g^{-1}, and 0.6 m^2g^{-1}, respectively. This indicated that both Cu/Al_2O_3 and Cu/Mont catalysts possessed higher surface area than other Cu-supported catalysts. The trend of surface area follows Cu/Al_2O_3 > Cu/Mont > Cu/Bent > Cu/Dol > Cu/Talc. Similarly, different catalyst supports had a substantial impact on catalyst pore volume. The high surface area of Cu/Al_2O_3 and Cu/Mont catalysts was correlated well with their high pore volume (>0.10 cm^3g^1) contributed from the enhancement of adsorbed volume of liquid nitrogen. Furthermore, different catalyst supports gave different pore diameters ranging from 19.07 to 61.21 Å. From Table 1, Cu/Dol, Cu/Al_2O_3 and Cu/Mont catalysts exhibited relatively similar pore diameter in the range 19.07–19.19 Å while bigger pore diameter was exhibited by Cu/Bent and Cu/Talc catalysts of 61.21 Å and 32.28 Å, respectively. Although Cu/Bent and Cu/Talc gave a bigger pore diameter but their pore volume were lower as the adsorption of liquid nitrogen could be on the external surface area and not micropore filling.

3.2. XRD

The XRD patterns for calcined and reduced sample are shown in Fig. 1(A) and Fig. 1(B), respectively. The addition of copper to all supports was indicated by the formation of the bulk CuO phase (JCPDS; 44–0706). The formation of bulk CuO crystalline was attributed to the agglomeration of Cu species in the catalyst (Putrakumar et al., 2015). Accordingly, the higher peak intensity of the CuO phase at 2θ = 35.6° and 38.8° were observed for all catalysts except for Cu/Dol catalyst which showed a rather small and broad peak. Meanwhile, the small diffraction peak of the CuO phase at 2θ = 48.8°, 61.4°, and 68.5° were detected for all catalysts except in Cu/Dol. This may be due to good dispersion copper oxide species on the dolomite surface by forming small size of particles thus hard to be detected. On the other hand, there was no characteristic peak related to any metallic Cu species observed in all Cu-supported catalysts.

Furthermore, for Cu/Al_2O_3 catalyst, the characteristic peak of Al_2O_3 support phases were detected at 2θ = 58.3° and 66.5°. For Cu/Dol catalyst, mixed crystalline phases of dolomite support components were detected. As such the diffraction peaks at 2θ = 18.1°, 28.3°, and 33.8° were corresponded to $CaMg_2$ alloy (JCPDS; 01–1070). The characteristic peaks attributed to $CaCO_3$ has 2θ = 29.3° and 33.2° (JCPDS; 01–1032). The peaks at 2θ = 37.5°, 62.2°, and 67.5° were due to the dolomite phase (JCPDS; 02–0767) while the peak at 2θ = 43.1° was assigned to $MgCO_3$ phase (JCPDS; 02–0871). The peaks for CaO phases were observed at 2θ = 54.3° and 64.2° (JCPDS; 01–1160). For Cu/Talc catalyst, the peak formation of $MgSiO_3$ phases was observed at 2θ = 28.3° and 30.5° (JCPDS; 02–0546), emphasizing that the talcum support consisted of a mixed metal oxide which is similar to findings reported by Maleki et al. (2017). For Cu/Bent and Cu/Mont, both catalysts were assigned with the presence of $Al_2O_3{\cdot}3H_2O$ (2θ = 19.5°), $Ca(AlO_2)_2$ (2θ = 26.8°), and Al_2O_3 phases (2θ = 58.5° and 66.5°), indicating bentonite and montmorillonite supports were enriched with the proportion of alumina and calcium species in the support component. In addition, based on the XRD patterns in Fig. 1(A), it was noted that the small and broad diffraction peaks of the Al_2O_3 phase centered at 2θ = 58.5° and 66.5° were noticeable in all Cu-supported catalysts except for Cu/Dol. Thus, it can be concluded

Table 1
Physicochemical properties of the catalysts.

Catalyst	BET			XRD		H_2-TPR		NH_3-TPD
	Surface area[a] (m^2g^{-1})	Pore volume[b] (cm^3g^{-1})	Pore diameter[b] (Å)	Average Cu crystallite size (nm)[c]	H_2 consumed at different temp[d] (μmol/g) 150–550 °C	Total amount H_2 consumed[d] (μmol/g) >550 °C	Total amount NH_3 adsorbed[e] (μmol/g)	>550 °C
Cu/Dol	9.7	0.098	19.07	58.2	23582, 17,919	10,268	51,769	19,528
Cu/Al_2O_3	34.5	0.328	19.15	70.6	9599, 26,160	–	35,759	4197
Cu/Bent	5.3	0.089	61.21	100.4	35,389	–	35,389	1992
Cu/Mont	30	0.270	19.19	100.4	18770, 13,875	–	32,645	3215
Cu/Talc	0.6	0.014	32.28	107.5	44,846	–	44,846	2890
Copper oxide	–	–	–	–	110	–	110	607

[a] Calculated using BET method.
[b] Calculated using BJH method.
[c] Calculated using Cu peak at 2θ = 43.29° (111), 50.42° (200), and 74.09° (220) by the Scherrer equation, crystallite size = 0.89λ/βcosθ, where λ = 0.15406 nm, β = full-width at half maximum (FWHM) and θ = Bragg angle.
[d] H_2-TPR peak for all catalysts.
[e] NH_3-TPD desorption peak for all catalysts.

that alumina species was also a constituent of bentonite, montmorillonite, and talcum support.

Meanwhile, the XRD pattern in Fig. 1(B) indicated that the CuO peaks (2θ = 35.5°, 38.5°, 48.8°, 61.4°, and 68.5°) of all calcined samples disappeared, while the peaks at 2θ = 43.2°, 50.4°, and 74.1° (JCPDS; 85–1326) corresponding to metallic copper species (Cu^0) emerged. The similar diffraction peak of metallic copper was also reported by Zhu et al. (2013) and Wen et al. (2013). The formation of metallic copper was as a result of the segregation of Cu clusters crystallite (Lin et al., 2012). In this study, it was noted that the H_2 reduction treatment on the calcined catalysts did significantly change the copper crystal structure as such three main peaks of Cu^0 with different planes of (111), (200) and (220) at 2θ = 43.29°, 50.42°, and 74.09° respectively were observed.

As seen in Fig. 1(B), the peak intensities of metallic Cu at 2θ = 43.81° (111), 50.84° (200), and 74.76° (220) were sharp for Cu/Talc, Cu/Bent and Cu/Mont catalysts. However, the metallic Cu peak in Cu/Dol and Cu/Al_2O_3 catalysts has a small and less intense peak, suggesting that the available copper species were inclined to aggregate into larger particles. This is in agreement with the smaller crystallite size of copper obtained for Cu/Dol and Cu/Al_2O_3 catalysts in Table 1. In contrast, the copper particle would tends to aggregate into larger particles when the interaction bonding between copper species and support material was weak (Zhu et al., 2013) and made it poor in metal dispersion.

Meanwhile, as established in literature, a metal oxide tended to form spinel when it was supported with clay or limestone material containing Mg and Al species (Kovanda et al., 2001). Apparently, in this study, the presence of Cu_2MgO_3 (JCPDS; 21–0291) (2θ = 35.3°, 37.5°, 38.2°, and 48°) and $CuAlO_2$ spinel phases (JCPDS; 09–0185) (2θ = 35.8°) were detected for Cu/Dol and Cu/Al_2O_3 catalyst, respectively. Also, it was found that no characteristic peak of any CuO and Cu_2O phase was observed in all reduced samples, assigning that the reduction of Cu^{2+} species at 600 °C was complete and metallic copper was successfully formed. Therefore, the interaction of copper species and the support materials were obviously influenced by the stability and redox properties of all Cu-supported catalysts as also reported by Zhao et al. (2013).

Apart from that, the average crystallite size of metallic Cu in Table 1 was in the range 50–100 nm. The smallest Cu crystallite of 58.2 nm was attained on Cu/Dol catalyst followed by Cu/Al_2O_3 with 70.6 nm. While Cu/Bent, Cu/Mont, Cu/Talc catalyst exhibited relatively larger sizes ~100 nm. The particles size of Cu increased as Cu/Dol < Cu/Al_2O_3 < Cu/Bent < Cu/Mont < Cu/Talc. The finding is also in agreement with Feng et al. (2008) who reported that different Ru particle sizes on different supports showed the intrinsic property of the support material. Nevertheless, the increase of particle size was defined as the aggregation of particle or particle sintering and this would inevitably lead to a decrease in catalyst activity due to poor metal dispersion.

3.3. H_2-TPR

The H_2-TPR profile of copper oxide sample and all Cu-supported catalysts is presented in Fig. 2 while the hydrogen consumption data is summarized in Table 1. From Fig. 2, Cu/Al_2O_3 and Cu/Dol catalysts showed peaks at a lower reduction temperature with respect to pure copper oxide sample that reduced at 338 °C with a shoulder at 428 °C. Apparently, all supported catalysts exhibited main reduction peak at temperature range of 200–400 °C, except for Cu/Dol catalyst which exhibited additional peaks at higher temperature. For Cu/Al_2O_3 catalyst, it essentially exhibited two peaks which partially overlapped at 251 °C and a broad shoulder at a higher temperature of 328 °C. Meanwhile, the Cu/Bent, Cu/Talc and Cu/Mont catalysts recorded only one desorption peak at 313, 364, and 369 °C, respectively. For Cu/Dol catalyst, three desorption peaks were observed at 298, 435, and 615 °C.

From previous studies, it was stated that the reduction of dispersed copper oxide species to metallic copper Cu^0 was effective at <250 °C (Zhao et al., 2017). Accordingly, the reduction of copper crystal phase (bulk CuO) was proposed to be reduced at a temperature higher than 250 °C (Wen et al., 2013). For higher reduction temperature (>400 °C), it was assigned to the reduction of the copper-support phase or copper in the spinel phase (Vargas-Hernández et al., 2014). In this study, the first reduction profile of all catalysts at ~200–300 °C were assigned to the two reduction of small and big clusters of CuO species to the metallic Cu species. It started from Cu^{2+} ions to Cu^+ ions ($CuO \rightarrow Cu_2O$), followed by a reduction of Cu^+ ions to metallic copper species ($Cu_2O \rightarrow Cu^0$) (Srivastava et al., 2017; Liu et al., 2016). Apparently, the first reduction profile of all supported catalysts coincided very well with the reduction peak of copper oxide sample which reduced in almost similar reduction temperature range ~250–400 °C.

Furthermore, Tanasoi et al. (2009) reported that that the broad reduction profiles of Cu-containing mixed oxides at 400–750 °C were credited to reduction of surface copper in aluminate spinel phases ($CuAl_2O_4$) or even due to more complex $Cu_xMg_xAl_2O_4$ phases. Moreover, the broad reduction peak derived from spinel phase was closely related to the interphase hydrogen adsorption. In this way, more hydrogen was presumably consumed among the metals (Li et al. 2009). As seen in Fig. 2, the TPR peak of Cu/Al_2O_3 catalyst (at 251 °C and 328 °C) emerges to be highly broad

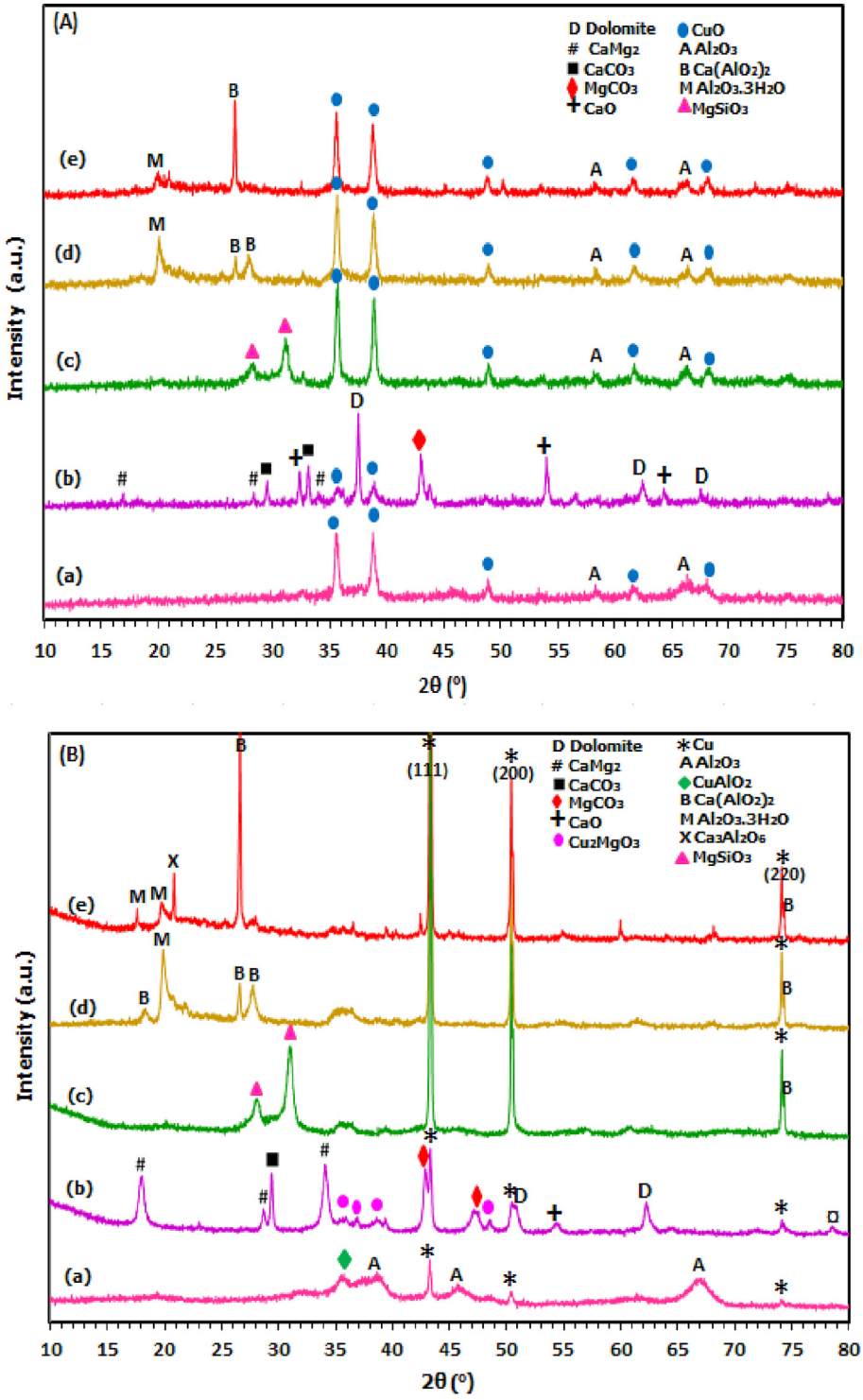

Fig. 1. XRD diffractograms of calcined (A) and reduced samples (B) for (a) Cu/Al_2O_3, (b) Cu/Dol, (c) Cu/Talc, (d) Cu/Bent and (e) Cu/Mont.

than other supported catalysts. This could be due to the presence of different copper species in alumina support or their spinel phases.

In the case of Cu/Dol catalyst, the three reduction peaks were smaller and lower than other supported catalysts or even copper oxide sample. This could be attributed to the presence of smaller copper particles and was consistent with the small particle size obtained for Cu/Dol in Table 1. Meanwhile, the formation of a second reduction peak at 455 °C corresponded to the reduction of copper cluster or copper oxide species in the interstitial defects due to the interaction with dolomite support since Cu_2MgO_3 spinel was indicated in XRD peak in Fig. 1. The peak at 639 °C could be correponded to the reduction of bulk dolomite support as this was similar in a finding by Azri et al. (2020). During reduction condition, CuO favored formation of oxygen vacancies by producing Cu^+ ions and on catalyst surface. The unstable Cu^+ ions was reduced to metallic Cu^0 by electron transfer (Maimaiti et al., 2014; Wen et al., 2013).

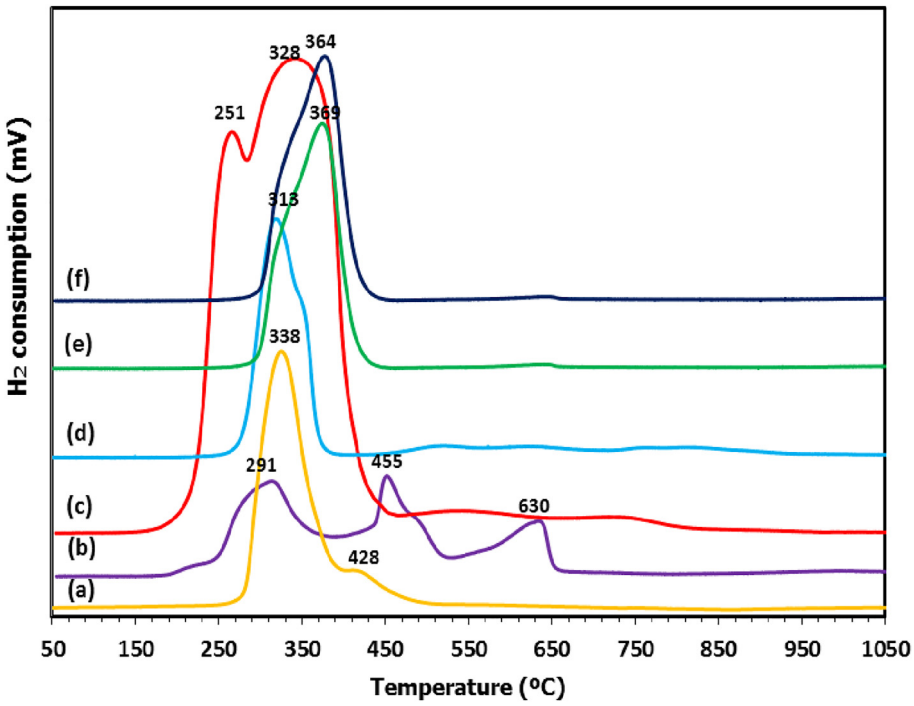

Fig. 2. H_2-TPR profiles of (a) Copper oxide, (b) Cu/Dol, (c) Cu/Al_2O_3, (d) Cu/Bent, (e) Cu/Mont and (f) Cu/Talc.

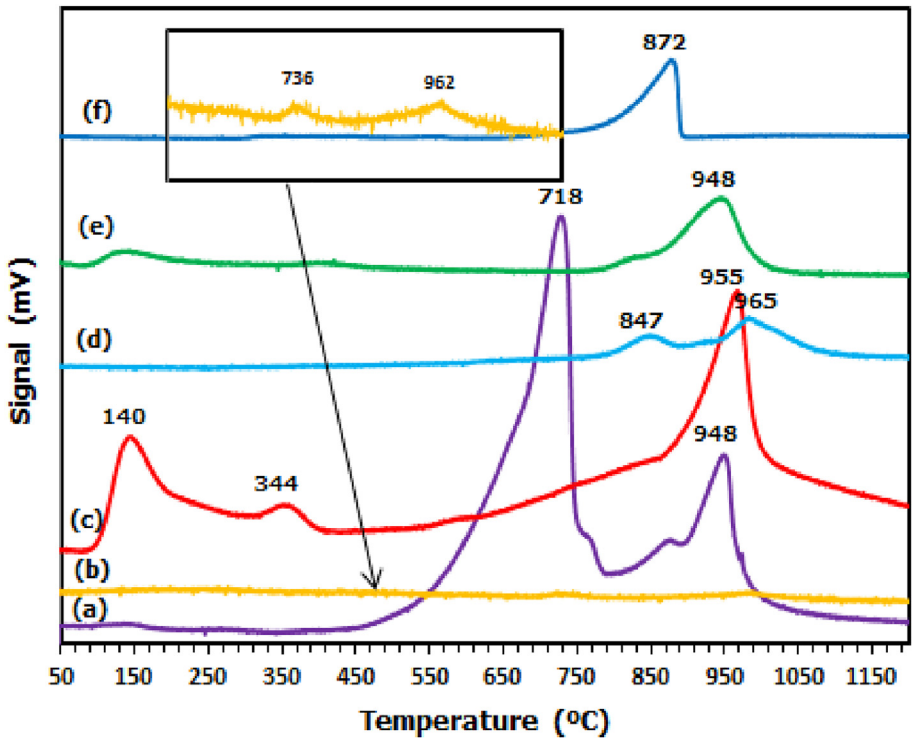

Fig. 3. NH_3-TPD profiles of (a) Cu/Dol, (b) Copper oxide, (c) Cu/Al_2O_3, (d) Cu/Bent, (e) Cu/Mont and (f) Cu/Talc.

For Cu/Bent, Cu/Mont, and Cu/Talc catalysts, the reduction peaks were essentially similar to copper oxide peak at ~330 °C, showing no significant change of metal reducibility. This was correlated to the findings from XRD analysis in Fig. 1 since no formation of copper in spinel was detected. Based on reduction profile, the reduction temperature increased in the order Cu/Al_2O_3 < Cu/Dol < Cu/Bent < copper oxide < Cu/Talc < Cu/Mont. The lower reduction temperature of Cu/Al_2O_3 and Cu/Dol catalysts than their copper oxide sample was due to the presence of copper in the spinel of which altered the reducibility of metal oxide species. Based on H_2 consumption data in Table 1, higher H_2 consumption was required for supported catalysts than the amount necessarily needed for the complete reduction of copper oxide due to higher surface exposure area. The H_2 consumption are ranked as Cu/Do

l > Cu/Talc > Cu/Al_2O_3 > Cu/Bent > Cu/Mont > copper oxide. Consequently, copper species was easily reduced using dolomite and alumina as catalyst supports in comparison to bentonite, montmorillonite, and talcum.

3.4. NH_3-TPD

The results of the ammonia desorption profile are shown in Fig. 3 while the corresponding acidity value (amount of ammonia uptakes) is tabulated in Table 1. All catalysts except Cu/Al_2O_3, exhibited desorption peaks above 500 °C, indicating the presence of strong acid sites on the catalyst surface. In the case of Cu/Al_2O_3 catalyst, desorption peaks were presented in all three acidic sites (weak, medium, and strong). Meanwhile Cu/Dol catalyst emerged as the highest and broadest peak (at 718 and 948 °C) among other supported catalysts. In contrast, Cu/Bent, Cu/Mont, Cu/Talc, and Cu/Al_2O_3 catalysts showed smaller and lower desorption peak at (847 and 965 °C), 948, and 872 °C, and (140, 344, and 955 °C), respectively. Copper oxide sample exhibited the smallest and lowest desorption peaks at 736 °C and 962 °C.

Notably, it was found that as copper oxide species was incorporated to support materials, the desorption peaks emerged broader and higher. It was due to the enhancement of copper content with catalyst support thus induced more ammonia desorption as well as the acid amount. Apparently, it was observed that the desorption peaks of Cu/Dol (~700 °C and ~950 °C) coincided very well with the desorption profile of copper oxide sample and simultaneously resulted in its highest acidity. This attributable to the strong impact of copper on the dolomite support and as an indication the copper was well dispersed over the dolomite surface than other supports. It is worth mentioning that the presence of carbonate content in dolomite support may be responsible for its highest acid sites amount (19528 μmol/g). The high acid sites in Cu/Dol catalyst act as active sites and contribute to high activation of the C-O bond

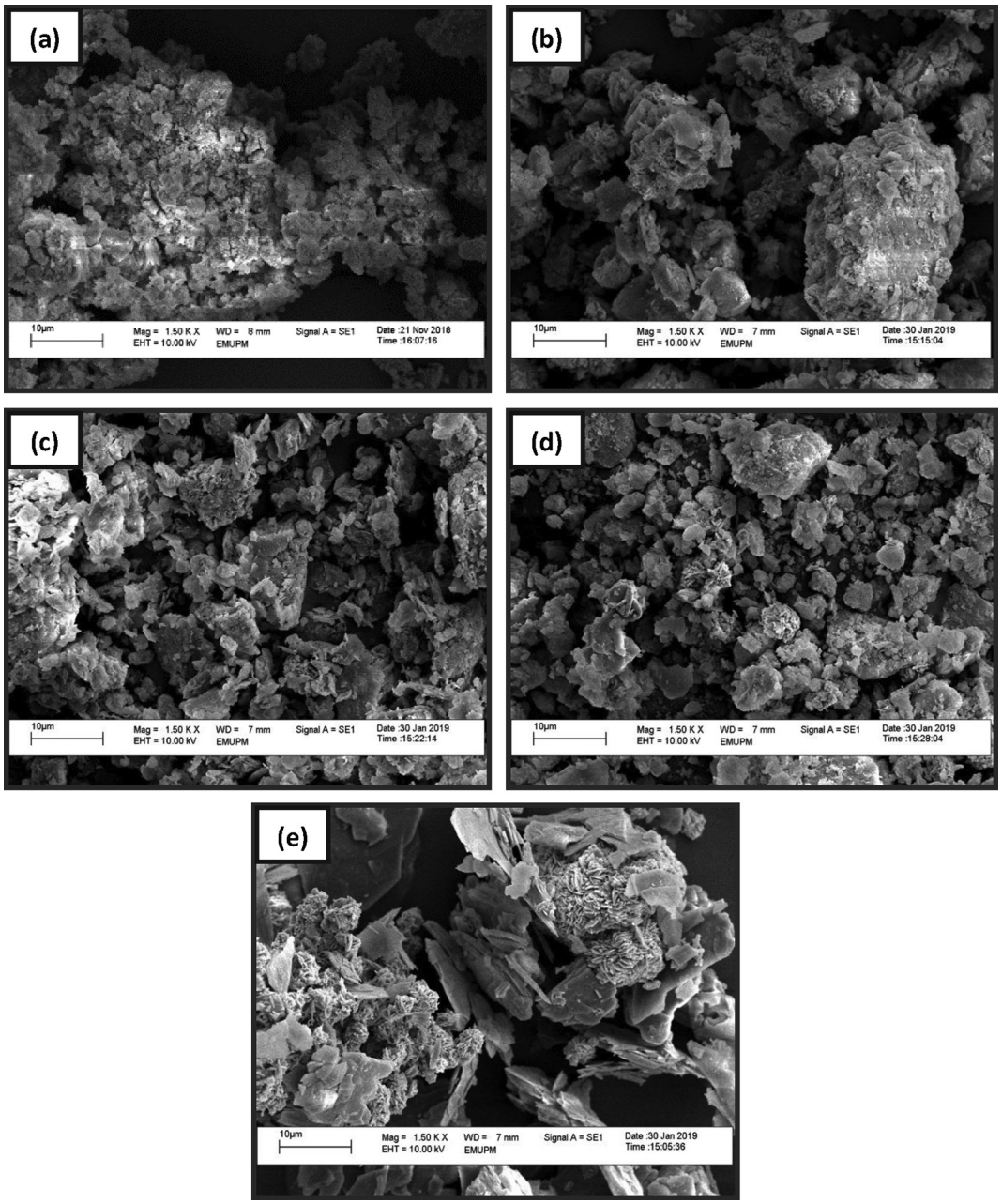

Fig. 4. SEM images of (a) Cu/Dol, (b) Cu/Al_2O_3, (c) Cu/Bent, (d) Cu/Mont and (e) Cu/Talc with 15000X magnification.

of glycerol during dehydration reaction and consequently improved the performance of glycerol hydrogenolysis.

3.5. SEM

The surface morphology of all Cu-supported catalysts in Fig. 4 illustrates that the individual grains segregation was hard to be identified. The particles displayed agglomerated structure with an irregular shape of an average size of 10 mm (from scale bar), emphasizing the formation of a macroporous solid in a cluster of closely spaced crystals. This was due to metal-support interaction from the incorporation of copper species to catalyst support in line with the presence of mixed crystalline phases shown in XRD analysis.

4. Catalytic hydrogenolysis

As shown in Table 2, the results clearly show very low glycerol conversion (8.7%) and no selectivity towards 1,2-PDO for the blank experiment. With the presence of catalysts in the reaction, a more pronounced effect was observed. Glycerol conversion of 22.6% was obtained with metallic copper, however, no selectivity to the desired product (1,2-PDO) was observed. It means that the metallic Cu alone was not capable to catalyze the hydrogenolysis reaction. The introduction of copper metal to different supports significantly influenced the progression of the reaction. Cu/Dol catalyst exhibited predominant activity by giving the highest glycerol conversion (78.5%) and selectivity to 1,2-PDO (79%) among other supported catalysts. While Cu/Al_2O_3, Cu/Talc, Cu/Bent and Cu/Mont catalysts resulted in lower glycerol conversion and 1,2-PDO selectivity of (28%, 66.8%), (72.3%, 43.5%), (68.8%, 14.6%) and (50%, 20%), respectively. The higher TOF value of Cu/Dol catalyst correlated with the high catalytic activity in glycerol hydrogenolysis.

Among all supported catalysts, Cu/Al_2O_3 and Cu/Mont catalysts exhibited quite low glycerol conversion of ($\leq$50%) while Cu/Bent and Cu/Mont catalysts exhibited low 1,2-PDO selectivity of ($\leq$20%). In the case of Cu/Mont catalyst, it exhibited poor activity in both glycerol conversion and 1,2-PDO selectivity. The glycerol conversion of all catalysts increased in the order Cu/Dol > Cu/Talc > Cu/Bent > Cu/Mont > Cu/Al_2O_3 > metallic copper. Meanwhile, the order of 1,2-PDO selectivity ranks as Cu/Dol > Cu/Al_2O_3 > Cu/Talc > Cu/Mont > Cu/Bent. The high glycerol hydrogenolysis exhibited by Cu/Dol catalyst agreed with its high surface acid sites as indicated in the NH_3-TPD profile (Fig. 3 and Table 1). During glycerol hydrogenolysis, glycerol was adsorbed, dehydrated and thus converted to acetol on acid sites. This subsequently transformed into 1,2-PDO. Accordingly, higher acidity provides a greater number of acid sites, thus a greater number of glycerol molecules could be dehydrated on the catalyst surface (Cu/Dol).

Next, the presence of a metallic site in a catalyst is very crucial for the glycerol hydrogenation reaction since it acted as reaction sites to facilitate the hydrogenation reaction. It helps in dissociating hydrogen gas into hydride and thus contributing to hydrogenation of intermediate (acetol) to 1,2-PDO. Accordingly, the formation of copper metallic sites in all catalysts was closely related to its reduction behaviour. In the case of Cu/Dol and Cu/Al_2O_3 catalysts, based on the H_2-TPR profile presented in Fig. 2, it showed that copper species of both catalysts were essentially reduced at lower reduction temperatures (291 °C and 251 °C) when compared with the others. Therefore, it is good that dolomite and Al_2O_3 could enhance the reducibility of copper species to lower temperature than pure copper oxide sample, and this might have contributed to the high 1,2-PDO selectivity obtained for both catalysts.

During catalytic reaction, the metal catalyst should remain in its reduced state (metallic state) to provide high metal sites for hydrogenation reaction to occur. Accordingly, the catalytic reaction conducted at 200 °C in this study agreed with the reducibility of copper species ($\geq$ ~200 °C). Therefore, the high 1,2-PDO selectivity of Cu/Dol and Cu/Al_2O_3 catalysts was due to the presence of metallic copper which is active within the reduction temperature of copper species ($\geq$200 °C). However, in the case of Cu/Bent, Cu/Mont and Cu/Talc catalysts, the presence metallic Cu species was suggested to be in the form of unstable reduced state since the metal reduction of the catalysts from H_2-TPR occurred at higher temperature of 313 °C, 369 °C, 364 °C, respectively. Thus, this corresponds to the lower 1,2-PDO selectivity obtained for the catalyst.

Meanwhile, the hydrogen adsorption (hydrogen activation) played an important role in determining a high catalytic hydrogenation reaction. As proposed by Ren et al. (2015), bigger Cu particles gave a low activity in hydrogenation of methanol over Cu-ZnO-ZrO_2-MgO/Al_2O_3 catalyst due to the low metal surface exposure for activating hydrogen on the catalyst surface. Similarly, higher 1,2-PDO selectivity for Cu/Dol and Cu/Al_2O_3 catalysts was related to their smaller Cu particles.

5. Conclusion

The Cu/Dol catalyst was found to exhibit a more pronounced effect with the highest conversion of glycerol and 1,2-PDO selectivity of 78.5% and 79%, respectively at a reaction temperature of 200 °C, pressure of 4 MPa and reaction time of 10 h. It was noted that the high acidity, high metal reducibility (easy reduction of copper species at lower reduction temperature), and small Cu particle were the factors that contributed to its high catalytic performance.

Declaration of Competing Interest

The authors declare that they have no known competing financial interests or personal relationships that could have appeared to influence the work reported in this paper.

Table 2
Catalytic activity of all catalysts.

Sample	Conversion (%)	Selectivity (%)			TOF (h^{-1})
		Acetol	1,2-PDO	Methanol	
Blank	8.7	0	0	0	–
Metallic copper	22.6	0	0	0	0.98
Cu/Dol	78.5	18.91	79	2.1	3.41
Cu/Al_2O_3	28	19.29	66.8	13.9	0.78
Cu/Talc	72.3	12.45	43.5	44.2	3.14
Cu/Bent	68.8	0	14.6	85.4	2.99
Cu/Mont	50	0	20	80	0.22

Catalytic reaction conditions: 20 ml aqueous glycerol (20 wt%); 200 °C reaction temperature; 4 MPa H_2 pressure; 1 g catalyst dosage; 10 h reaction time.

Acknowledgments

The authors wish to acknowledge the financial grant supported by Universiti Putra Malaysia for Geran Inisiatif Putra Siswazah (GP-IPS/2018/9619500) in support of the project.

References

Azri, N., Ramli, I., Nda-Umar, U.I., Shamsuddin, M.R., Saiman, M.I., Taufiq-Yap, Y.H., 2020. Copper-dolomite as effective catalyst for glycerol hydrogenolysis to 1,2-propanediol. J. Taiwan Inst. Chem. Eng.

Feng, J., Fu, H., Wang, J., Li, R., Chen, H., Li, X., 2008. Hydrogenolysis of glycerol to glycols over ruthenium catalysts: Effect of support and catalyst reduction temperature. Catal. Commun. 9, 1458–1464.

Freitas, I.C., Manfro, R.L., Souza, M.M.V.M., 2018. Hydrogenolysis of glycerol to propylene glycol in continuous system without hydrogen addition over Cu-Ni catalysts. Appl. Catal. B, Environ. 220, 31–41.

Kovanda, F., Jiratova, K., Rymes, J., Kolousek, D., 2001. Characterization of activated Cu/Mg/Al hydrotalcites and their catalytic activity in toluene combustion. Appl. Clay Sci. 18, 71–80.

Li, Y., Guo, Y., Xue, B., 2009. Catalytic combustion of methane over M (Ni Co, Cu) supported on ceria-magnesia. Fuel Process. Technol. 90, 652–656.

Lin, J., Zhao, X., Cui, Y., Zhang, H., Liao, D., 2012. Effect of feedstock solvent on the stability of Cu/SiO_2 catalyst for vapor-phase hydrogenation of dimethyl oxalate to ethylene glycol. Chem. Commun. 48, 1177–1179.

Liu, L., Lou, H., Chen, M., 2016. Selective hydrogenation of furfural to tetrahydrofurfuryl alcohol over Ni/CNTs and bimetallic CueNi/CNTs catalysts. Int. J. Hydrogen Energy 41, 14721–14731.

Liu, Y., Guo, X., Rempel, G.L., Ng, F.T.T., 2019. The promoting effect of Ni on glycerol hydrogenolysis to 1,2-Propanediol with in situ hydrogen from methanol steam reforming using a $Cu/ZnO/Al_2O_3$ catalyst. Catalysts 9, 412.

Maimaiti, Y., Nolan, M., Elliott, S.D., 2014. Reduction mechanisms of the CuO(111) surface through surface oxygen vacancy formation and hydrogen adsorption. Phys. Chem. 16, 3036–3046.

Maleki, H., Kazemeini, M., Bastan, F., 2017. Transesterification of canola oil to biodiesel using CaO/Talc nanopowder as a mixed oxide catalyst. Chem. Eng. Technol. 40, 1923–1930.

Mallesham, B., Sudarsanam, P., Reddy, B.V.S., Reddy, B.M., 2016. Development of cerium promoted copper – magnesium catalysts for biomass valorization: Selective hydrogenolysis of bioglycerol. Appl. Catal. B Environ. 181, 47–57.

Putrakumar, B.; Nagaraju, N.; Kumar,V. P.; Chary, K.V.R., 2015. Hydrogenation of levulinic acid to valerolactone over copper catalysts supported on Al2O3. 250, 209–217.

Ren, H., Xu, C., Zhao, H., Wang, Y., Liu, J., Liu, J., 2015. Methanol synthesis from CO_2 hydrogenation over $Cu/g\text{-}Al_2O_3$ catalysts modified by ZnO, ZrO_2 and MgO. J. Indu. Eng. Chem. 28, 261–267.

Soares, A.V.H., Salazar, J.B., Falcone, D.D., Vasconcellos, F.A., Davis, R.J., Passos, F.B., 2016. A study of glycerol hydrogenolysis over $Ru–Cu/Al_2O_3$ and $Ru–Cu/ZrO_2$ catalysts. J. Mol. Catal. A, Chem. 415, 27–36.

Srivastava, S., Jadeja, G.C., Parikh, J., 2017. Synergism studies on alumina-supported copper nickel catalysts towards furfural and 5-hydroxymethylfurfural hydrogenation. J. Mol. Catal. A Chem. 426, 244–256.

Tanasoi, S., Tanchoux, N., Adriana, U., Tichit, D., Sandulescu, I., Fajula, F., Marcu, I.C., 2009. New Cu-based mixed oxides obtained from LDH precursors, catalysts for methane total oxidation. Appl. Catal. A Gen. 363, 135–142.

Vargas-Hernández, D., Rubio-Caballero, J.M., Santamaría-González, J., Moreno-Tost, R., Mérida Robles, J.M., Pérez-Cruz, M.A., Jiménez-López, A., Hernández-Huesca, R., Maireles-Torres, P., 2014. Furfuryl alcohol from furfural hydrogenation over copper supported on SBA-15 silica catalysts. J. Mol. Catal. A Chem. 383–384, 106–113.

Wen, C., Yin, A., Cui, Y., Yang, X., Dai, W.-L., Fan, K., 2013. Enhanced catalytic performance for $SiO_2–TiO_2$ binary oxide supported Cu-based catalyst in the hydrogenation of dimethyloxalate. Appl. Catal. A: Gen. 458, 82–89.

Zhao, S., Yue, H., Zhao, Y., Wang, B., Geng, Y., Lv, J., Wang, S., Gong, J., Ma, X., 2013. Chemoselective synthesis of ethanol via hydrogenation of dimethyl oxalate on Cu/SiO_2: Enhanced stability with boron dopant. J. Catal. 297, 142–150.

Zhao, Y., Zhang, Y., Wang, Y., Zhang, J., Xu, Y., Wang, S., Ma, X., 2017. Structural evolution of mesoporous silica supported copper catalyst for dimethyl oxalate hydrogenation. Appl. Cat. A Gen. 539, 59–69.

Zhu, S., Gao, X., Zhu, Y., Zhu, Y., Zheng, H., Li, Y., 2013. Promoting effect of boron oxide on Cu/SiO_2 catalyst for glycerol hydrogenolysis to 1,2-propanediol. J. Catal. 303, 70–79.